Nonlinear Dyn (2022) 107:1003–1021
https://doi.org/10.1007/s11071-021-07004-y

ORIGINAL PAPER

H_∞ non-clutch coordinated control for mode transition system of DM-PHEV with CAN-induced delays

Cong Liang · Xing Xu · Feng Wang · Zhiguang Zhou

Received: 17 July 2021 / Accepted: 17 October 2021 / Published online: 15 November 2021

Abstract Considering the effects of asynchronous controller area network (CAN)-induced random delays in the control system of a dual motor plug-in hybrid electric vehicle (DM-PHEV), a robust H_∞ non-clutch coordinated controllers of mode transition process (MTP) are developed in this paper. A novel non-clutch coordinated control strategy which avoids the clutch slipping stage is proposed based on the structural characteristics of dual motors. Besides, by analyzing the characteristics of asynchronous CAN-induced random delays (ACDs) caused by the multiple actuators of DM-PHEV, complex nonlinearities of ACDs are modeled by convex polytope. Two different H_∞ non-clutch coordinated controllers are proposed to ensure the performance of MTP with ACDs. One controller considers that the control signal transmitted by CAN bus is derivative of torque, and the other controller considers the signal as torque. Comparative simulation and hardware-in-the-loop (HiL) test are provided to demonstrate the performance of MTP controlled by proposed controllers.

Keywords Network-induced delays · Non-clutch coordinated strategy · PHEV · Mode transition process · H_∞

C. Liang · X. Xu (✉) · F. Wang
Automotive Engineering Research Institute, Jiangsu University, Jiangsu 212013, Zhenjiang, People's Republic of China
e-mail: xuxing@ujs.edu.cn

C. Liang · X. Xu · F. Wang
Jiangsu Province Engineering Research Center of Electric Drive System and Intelligent Control for Alternative Vehicles, Zhenjiang 212013, China

Z. Zhou
New Energy Development Department Powertrain Technology Center, Chery Automobile Company, Wuhu, People's Republic of China

Nomenclature

CAN	Controller area network
MTP	Mode transition process
HiL	Hardware-in-the-loop
PHEV	Plug-in hybrid electric vehicle
HM	Hybrid electric vehicle
EV	Electric vehicle
ECU	Electronic control unit
TCU	Transmission control unit
LMI	Linear matrix inequality
RCAT	Robust H_∞ coordinated controller with torque as control signal
T_e	Torque of engine
θ_e	Angular displacement of engine shaft
k_{em}	Equivalent torsional stiffness between engine and motor 1
θ_{m1}	Angular displacement of motor 1 shaft
J_{m1}	Equivalent inertia moment of motor 1
c_{ml}	Equivalent damping coefficient between motor 1 and clutch
T_c	Torque transmitted by clutch

J_{cr}	Equivalent inertia moment of clutch driving disk
k_{rg}	Equivalent torsional stiffness between clutch and gear g2
θ_{g2}	Angular displacement of the shaft of gear g2
J_{m2}	Equivalent inertia moment of motor 2
k_{m2}	Equivalent torsional stiffness between motor 2 and gear g1
θ_{g1},θ_{g2}	Angular displacement of the shaft of gear g1 and gear g2
J_{g1},J_{g2}	Equivalent inertia moment of gear g1 and g2
c_g	Equivalent damping coefficient between gear g1 and g2
c_{gr}	Equivalent damping coefficient between gear g2 and r1
J_{r1},J_{r2}	Equivalent inertia moment of gear r1 and r2
J_{f1},J_{f2}	Equivalent inertia moment of gear f1 and f2
θ_{f1},θ_{f2}	Angular displacement of the shaft of gear f1 and gear f2
c_r	Equivalent damping coefficient between gear r1 and r2
c_{rf}	Equivalent damping coefficient between gear r2 and f1
c_f	Equivalent damping coefficient between gear f1 and f2
c_w	Equivalent damping coefficient between gear f2 and wheel
J_w	Equivalent inertia moment of wheel
T_L	Equivalent running resistance torque of vehicle
A	Effective frontal area
m_{veh}	Vehicle mass
R	Radius of tire
k_{wv}	Equivalent torsional stiffness between vehicle body and wheel
i_0	Final drive ratio
i_2	Reduction ratio of motor 2
j_i	Priority of CAN message
l	Maximum length of frame
t_j	Period of jth priority CAN message
DM-PHEV	Dual-motor plug-in hybrid electric vehicle
ACD	Asynchronous CAN-induced random delays
HEV	Hybrid electric vehicle
EM	Electric driving mode
TDS	Torsional damping spring
LQR	Linear quadratic regulator
MCU	Motor control unit
HCU	Hybrid control unit
RHCC	Robust H_∞ coordinated controller
RCAD	Robust H_∞ coordinated controller with torque derivative as control signal
J_e	Moment of inertia of engine
θ_{m1}	Corner of motor 1 shaft
c_{em}	Equivalent damping coefficient between engine and motor 1
T_{m1}	Torque of motor 1
k_{ml}	Equivalent torsional stiffness between motor 1 and clutch
θ_l	Angular displacement of clutch-driven disk shaft
J_{cl}	Equivalent inertia moment of clutch-driven disk
θ_r	Angular displacement of clutch driving disk shaft
c_{rg}	Equivalent damping coefficient between clutch and gear g2
T_{m2}	Torque of motor 2
θ_{m2}	Angular displacement of the shaft of motor 2
c_{m2}	Equivalent damping coefficient between motor 2 and gear g1
r_{g1},r_{g2}	Radius of gear g1 and g2
k_g	Meshing stiffness between gear g1 and g2
k_{gr}	Meshing stiffness between gear g2 and r1
r_{r1},r_{r2}	Radius of gear r1 and r2
r_{f1},r_{f2}	Radius of gear f1 and f2
θ_{r1},θ_{r2}	Angular displacement of the shaft of gear r1 and gear r2
k_r	Meshing stiffness between gear r1 and r2
k_{rf}	Meshing stiffness between gear r2 and f1
k_f	Equivalent torsional stiffness between gear f1 and f2
k_w	Equivalent torsional stiffness between gear f2 and wheel
θ_w	Angular displacement of the shaft of wheel
θ_v	Angular displacement of the shaft of vehicle
C_d	Air drag coefficient
v	Speed of vehicle
f	Roll resistance coefficient
α	Road slope
c_{wv}	Equivalent damping coefficient between vehicle body and wheel

x_{is}^{ref}	Steady reference state signals
B_a	Linearization coefficient of air drag resistance torque
d	Measurement noise of sensors
R_a	Transmission rate of CAN network

1 Introduction

Hybrid electric vehicles (HEVs) are developed as the key to energy conservation and emission reduction. For plug-in hybrid electric vehicles (PHEVs) with large battery capacity, better fuel economy can be acquired [1–3]. Torque distribution and mode transition are the main tasks for controllers of PHEV to achieve high efficiency and optimal fuel economy [4,5]. Mode transition process (MTP) always includes power source access or exits, such as engine start/off or clutch engagement/disengagement, which may cause driveline vibration if the actuators are not well coordinated. Therefore, a coordinated control strategy for MTP should be designed to guarantee the drivability of PHEV [6–9].

MTP from electric driving mode (EM) to hybrid driving mode (HM) including engine start stage and clutch engagement stage is widely researched for its complicated architecture. For PHEVs with the engine directly connected to the output shaft through a torsional damper spring (TDS), the vehicle jerk is mainly caused by the engine ripple torque [10,11]. Thus, motors are used to compensate the unbalanced torque for its fast response speed [5,12]. For MTP of PHEV with the engine connected to the output shaft with a clutch, the engine ripple torque is blocked by the clutch on the side of clutch-driven disk. The performance of MTP mainly depends on the quality of clutch engagement [13,14]. Xu et at. pre-designed different reference trajectories of clutch engagement for various situations of engine start [15]. Smoothly trajectory of clutch engagement is proposed for comfortable start of engine, while steeply trajectory of clutch engagement is for quick start of engine. Besides, a controller for good tracking capability is also designed. However, it is difficult to acquire optimal results with the pre-designed trajectory. In addition to vehicle jerk which is usually used to evaluate the driver comfort, transient torsional oscillation is introduced to improve the fatigue life of planetary hybrid power-split system [16]. Considering parameters uncertainties and external disturbance, Yang et al. proposed two robust H_∞ controllers including upper layer which calculated the demand clutch torque and lower layer which performed the accurate position tracking control of clutch [17]. In the upper layer controller, both vehicle jerk and slipping energy loss are considered.

Normally, the engine is started by the slip of clutch, but this also brings additional energy consumption (slipping energy loss) and shorten the service life of clutch. For the dual motor plug-in hybrid electric vehicle (DM-PHEV) studied in this paper, the dual motors are located on both sides of the clutch; a non-clutch coordinated control strategy is firstly proposed. The engine can be started by the auxiliary motor connected to the clutch-driven disk. At the same time, the auxiliary motor can adjust the speed of both ends of the clutch to be synchronized, thereby skipping the clutch slipping stage and realizing the direct engagement of the clutch.

All of these studies of MTP assumed that the communications between controllers, actuators and sensors are instantaneous. Compared with traditional vehicles and electric vehicles (EVs), PHEVs have more actuators, sensors and control units. The communication between controllers of vehicle is realized by controller area network (CAN) bus. CAN is an industry standard broadly used for the communication among controllers, sensors and actuators [18]. However, the network bandwidth limitations in vehicle will inevitably lead to CAN-induced delays. Besides, the intelligentization of cars leads to the increasing burden in signal transmission, which will also induce random network delays [19–21]. For vehicle system with CAN-induced delays, the random delays can be described as uncertain time-delay system. Robust control strategy is widely applied in system with uncertainty. Many researches have been conducted on vehicle with random network delay. Luan et al. presented an adaptive model predictive control algorithm for uncertain model to solve the steering angle oscillation of autonomous vehicle caused by random network delays [22]. Liu et al. proposed a robust mixed H_∞/LQR tracking controller for integrated motor-transmission systems of EV with the CAN-induced delays [23]. Zhu et al. modeled the random network-induced delays as homogeneous Markov chains and developed a H_∞ controller to guarantee vehicle stability of EV [24].

Most of these aforementioned control methods focus on the effects of synchronous CAN-induced delays.

However, multiple power sources of PHEV with their own controllers are individual communication nodes on the CAN bus. Messages are transmitted sequentially according to communication priorities determined by the protocol. Due to the limitation of transmission rate, different communication priorities of multi-actuators lead to asynchronous CAN-induced random delays (ACDs). The performance of MTP may be seriously deteriorated by the incoordination of actuators caused by ACDs. Consequently, the ACDs in MTP system should be modeled and considered for the coordinated controller design in the PHEVs.

In this paper, H_∞ non-clutch coordinated controllers considering ACDs are proposed to minimize the vehicle jerk and mode transition time for MTP system with CAN-induced random delays. One controller considers that the control signal transmitted by CAN bus is derivative of torque, which is called RCAD controller. The other controller considers the signal as torque, which is called RCAT controller. The main contributions of this paper are summarized as follows.

(1) Based on the characteristics of DM-PHEV, non-clutch coordinated control strategy which helps to avoid energy loss caused by clutch slipping is firstly proposed.
(2) Due to the multiple actuators of DM-PHEV, ACDs that exist in MTP system are analyzed and mathematical model of MTP system with ACDs is built.
(3) The robust H_∞ output feedback controller is adopted to deal with the problems brought by asynchronous CAN-induced random delays to improve the performance of MTP of DM-PHEV.
(4) Two coordinated controllers based on different control signals are proposed: RCAT and RCAD controller assume the control signals as torque and torque derivative of actuators, respectively.

The rest of this paper is constructed as follows. In Sect. 2, a plant model of DM-PHEV is built. Problem formulation of MTP with ACDs and non-clutch coordinated control strategy are presented in Sect. 3. Section 4 gives the mathematical models of DM-PHEV with ACDs and the complex nonlinearities caused by ACDs are modeled by convex polytope. Coordinated controllers considering ACDs are also designed in Sect. 4. Results of Simulation and HiL tests are analyzed in Sect. 5. The conclusion is given in Sect. 6.

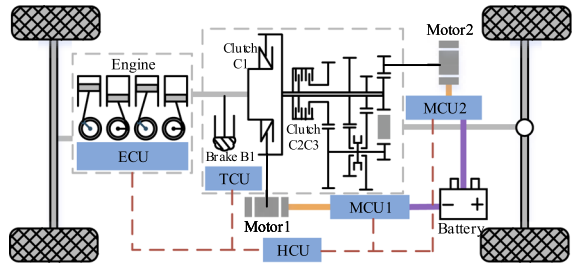

Fig. 1 Schematic diagram of the DM-PHEV

2 Modeling of DM-PHEV power-train

The architecture of DM-PHEV is shown in Fig. 1. The hybrid transmission consists of one engine, two motors, one brake and three clutches. Clutch C1 combines the power from engine and motor 1. Motor 1 can also be used as a start motor to start engine through the engaged clutch C1. Brake B1 is used to lock the engine. Clutch C2/C3 is connected with different gears of transmission. Engaged clutch C2/C3 combines the power from engine, motor 1 and motor 2. Through the disengagement/engagement of clutches and brake, the power of actuators can be disconnected/transmitted to the powertrain and achieve different working modes.

The actuators of DM-PHEV all have its own controllers. Electronic control unit (ECU) is the controller of engine. Motor control unit (MCU) is the controller of motor. Transmission control unit (TCU) is the controller of transmission and hybrid control unit (HCU) is the controller of vehicle. The controllers communicate through the CAN bus.

The components of power-train can be assumed as rigid bodies by ignoring the damping of each component. And the rotational inertia of each component is replaced by nodes with concentrated inertia. Then, the power-train of DM-PHEV can be modeled as Fig. 2.

The dynamic equation of engine can be described by

$$T_e - J_e\ddot{\theta}_e = T_{em} \tag{1}$$

where

$$T_{em} = k_{em}\left(\theta_e - \theta_{m1}\right) + c_{em}\left(\dot{\theta}_e - \dot{\theta}_{m1}\right) \tag{2}$$

The dynamic equation of motor 1 can be described by

$$T_{em} + T_{m1} - T_{ml} = J_{m1}\ddot{\theta}_{m1} \tag{3}$$

where

$$T_{ml} = k_{ml}\left(\theta_{m1} - \theta_l\right) + c_{ml}\left(\dot{\theta}_{m1} - \dot{\theta}_l\right) \tag{4}$$

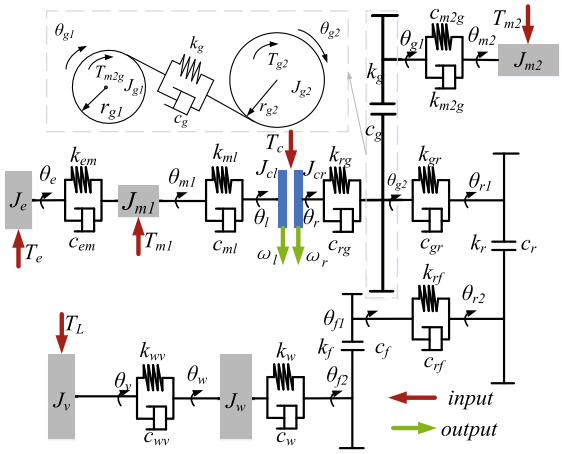

Fig. 2 Dynamic model of DM-PHEV

The equilibrium equation of clutch C2 can be described by

$$\begin{cases} T_c - T_{ml} = J_{cl}\ddot{\theta}_l \\ -T_c + T_{rg} = J_{cr}\ddot{\theta}_r \end{cases} \tag{5}$$

where

$$T_{rg} = k_{rg}\left(\theta_{g2} - \theta_r\right) + c_{rg}\left(\dot{\theta}_{g2} - \dot{\theta}_r\right) \tag{6}$$

The equilibrium equation of motor 2 can be derived as

$$T_{m2} - T_{m2g} = J_{m2}\ddot{\theta}_{m2} \tag{7}$$

where

$$T_{m2g} = k_{m2}\left(\theta_{m2} - \theta_{g1}\right) + c_{m2}\left(\dot{\theta}_{m2} - \dot{\theta}_{g1}\right) \tag{8}$$

The equilibrium equation of transmission gears may be given as

$$\begin{cases} T_{m2g} - r_{g1}T_g = J_{g1}\ddot{\theta}_{g1} \\ T_{rg} + r_{g2}T_g - T_{gr} = J_{g2}\ddot{\theta}_{g2} \\ T_{rg} + r_{g2}T_g - T_{gr} = J_{g2}\ddot{\theta}_{g2} \end{cases} \tag{9}$$

where

$$\begin{cases} T_g = k_g\left(r_{g1}\theta_{g1} - r_{g2}\theta_{g2}\right) \\ + c_g\left(r_{g1}\dot{\theta}_{g1} - r_{g2}\dot{\theta}_{g2}\right) \\ T_{gr} = k_{gr}\left(\theta_{g2} - \theta_{r1}\right) + c_{gr}\left(\dot{\theta}_{g2} - \dot{\theta}_{r1}\right) \end{cases} \tag{10}$$

The equilibrium equations of wheels can bebreak described by

$$\begin{cases} T_{gr} - r_{r1}T_r = J_{r1}\ddot{\theta}_{r1}, r_{r2}T_r - T_{rf} = J_{r2}\ddot{\theta}_{r2} \\ T_{rf} - r_{f1}T_f = J_{f1}\ddot{\theta}_{f1}, r_{f2}T_f - T_w = J_{f2}\ddot{\theta}_{f2} \end{cases} \tag{11}$$

where

$$\begin{cases} T_r = k_r\left(r_{r1}\theta_{r1} - r_{r2}\theta_{r2}\right) + c_r\left(r_{r1}\dot{\theta}_{r1} - r_{r2}\dot{\theta}_{r2}\right) \\ T_{rf} = k_{rf}\left(\theta_{r2} - \theta_{f1}\right) + c_{rf}\left(\dot{\theta}_{r2} - \dot{\theta}_{f1}\right) \\ T_f = k_f\left(r_{f1}\theta_{f1} - r_{f2}\theta_{f2}\right) \\ + c_f\left(r_{f1}\dot{\theta}_{f1} - r_{f2}\dot{\theta}_{f2}\right) \\ T_w = k_w\left(\theta_{f2} - \theta_w\right) + c_w\left(\dot{\theta}_{f2} - \dot{\theta}_w\right) \end{cases} \tag{12}$$

The equilibrium equation for the vehicle can be written as

$$\begin{cases} T_w - T_{wv} = J_w\ddot{\theta}_w, T_{wv} = J_v\ddot{\theta}_v + T_L \\ \frac{T_L}{R_t} = \frac{C_d A}{21.15}v^2 + m_{veh}gf\cos\alpha + m_{veh}g\sin\alpha \end{cases} \tag{13}$$

where

$$T_{wv} = k_{wv}\left(\theta_w - \theta_v\right) + c_{wv}\left(\dot{\theta}_w - \dot{\theta}_v\right) \tag{14}$$

The models of actuators and the main parameters have been built in the previous work [25].

3 Problem formulation of mode transition process

3.1 MTP of DM-PHEV

The MTP of DM-PHEV from EM to HM includes the start of engine and the engagement of clutch. In order to acquire a fast and smooth MTP, a coordinated control strategy is required. The performance indexes of MTP can be summarized as:

1) Torque demand: The MTP should avoid power shortage or even power interruption. The torque demand can be transformed into the tracking of the reference speed of the clutch driving disk.
2) Ride comfort of passengers: The transition of power may cause torque fluctuation and deteriorate the ride comfort of passengers. Vehicle jerk $j = \ddot{v}$ is used as the evaluation index.
3) Time of MTP: During MTP, the operating point of the actuators may not be within the high efficiency range. Thus, the time of MTP should be minimized to acquire optimal energy consumption.

3.2 Non-clutch control strategy

As shown in Fig. 3, the MTP of DM-PHEV can be divided into four stages. Stage 1 is Electric Driving Stage. The DM-PHEV is driven by motor 2 and clutch C2 in Fig. 1 keeps released. If a mode transition command is given by energy management controller, then vehicle begins MTP from EM to HM. DM-PHEV runs into Stage 2, Engine Start Stage. During Stage 2, clutch remains disengaged to avoid the transmission of torque fluctuations caused by engine start, and motor 1 works to start the engine. After engine speed ω_e exceeds the

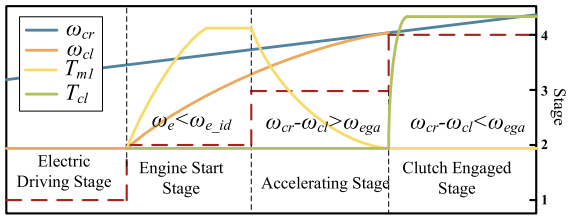

Fig. 3 Mode transition process of DM-PHEV

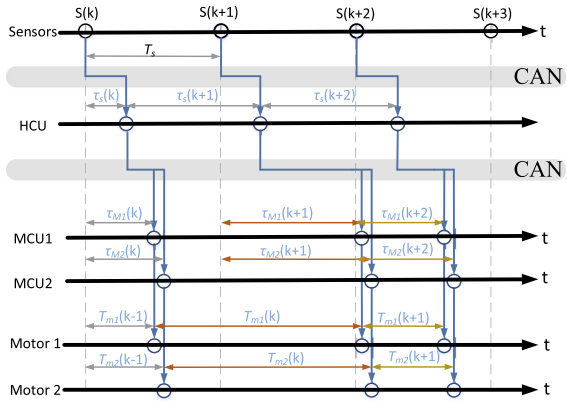

Fig. 4 Signal transmission of DM-PHEV over CAN

idle speed ω_{e_id}, MTP comes into Stage 3, Accelerating Stage. Since the clutch-driven disk of the clutch C2 of the DM-PHEV is connected to the motor 1, the output torque of the motor 1 T_{m1} can replace the slip of the clutch to realize the engagement of the clutch. The motor 1 accelerates the speed of the clutch-driven disk ω_{cl} to synchronize with the speed of the clutch driving disk ω_{cr}. Since there is no slip of clutch, the torque transmitted by clutch T_{cl} is zero. If $\omega_{cr} - \omega_{cl} < \omega_{ega}$ (ω_{ega} is a predefined speed difference threshold), then MTP runs into Stage 4, Clutch Engaged Stage.The torque of clutch T_{cl} increases rapidly and the clutch is directly engaged. The torque transmitted by clutch in Stage 4 is the combined torque of engine and motor 1. To avoid the sudden changes in the torque of output shaft at the moment of clutch engagement, the combined torque of Motor 1 and engine should be closed to zero in the end of Stage 3. This control strategy avoids clutch slip, so it is called non-clutch control strategy. The proposed non-clutch coordinated control strategy can achieve a more stable and economy mode switching process.

3.3 CAN-induced asynchronous random delays of MTP system

A communication network for the coordinated control system of MTP is usually constructed as shown in Fig. 4. Since the torque of the engine and the clutch is not controlled in the non-clutch coordinated control strategy, the delay information of the engine and the clutch is not displayed in Fig. 4. The states of DM-PHEV are measured by sensor node which works in time-driven mode. Because of the CAN-induced delays, the measurement signals are sent to HCU via CAN bus after a delay $\tau_s(k)$. Then, the HCU calculates the demand torque of actuators according to the proposed coordinated controller in event-driven mode. Afterward, the control signals are sent to MCU node in turn through the CAN bus. This process may introduce extra asynchronous random delays and cause excessive torque of motor 1 at the end of stage 3, which may cause vehicle jerk when clutch is engaged. So, a coordinated control strategy considering the effects of ACDs is necessary.

4 H_∞ non-clutch coordinated control strategy of DM-PHEV

The architecture of non-clutch coordinated control strategy is shown in Fig. 5. Once the MTP order is given by the upper layer controller, the DM-PHEV runs into MTP. Firstly, the stage of MTP is judged. Then, the reference speed signal is determined according to the current stage. The robust H_∞ non-clutch coordinated controller is designed in four steps. Firstly, mathematical model of MTP and CAN-induced random delays is built. Then, the random delays are characterized as uncertainties. In step 3, Taylor series expansion is adopted for linearization. Finally, a H_∞ controller is designed and the output feedback gain is obtained by solving the LMI problem.

4.1 Mathematical model of DM-PHEV during MTP

To effectively control the mode transition process of DM-PHEV, a simplified dynamic model is necessary. According to [26], the high frequency vibrations can be isolated effectively by the passive dampers. Thus, the driver comfort of vehicle is mainly related to the first

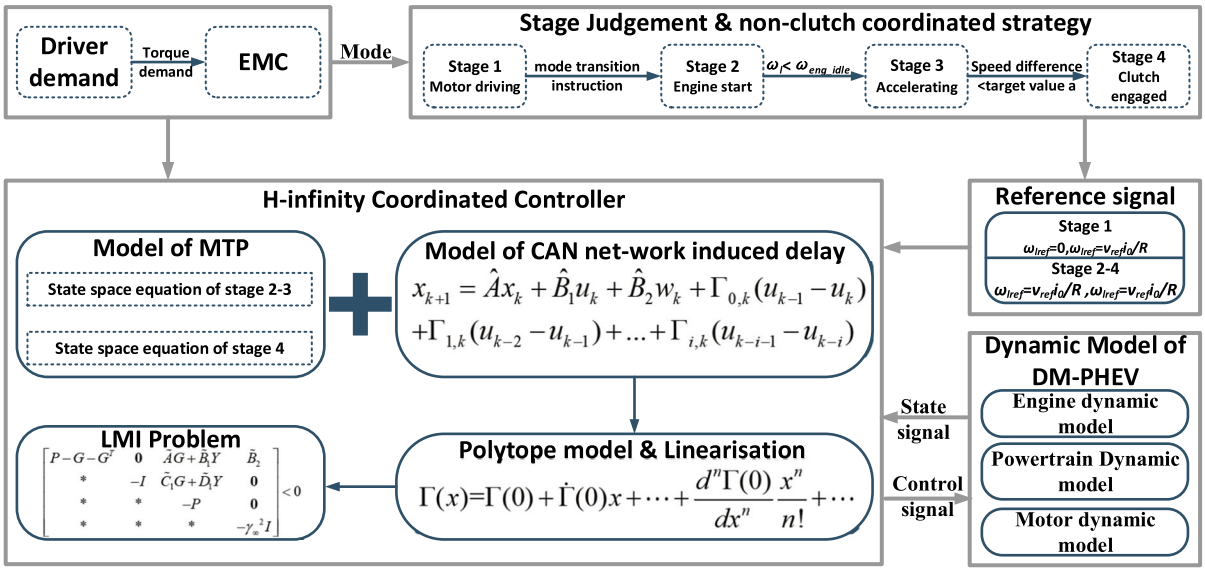

Fig. 5 Coordinated control architecture

two natural frequencies. In order to make the simplified model accurately describe the dynamic response of the system, the stiffness which has great influence on the first two order natural frequencies cannot be simplified. Here, the sensitivity of the natural frequency to the stiffness of the system is analyzed according to [26] and the results show that the sensitivity of the first two natural frequencies to the stiffnesses of input shaft and output shaft exceeds the others. Thus, only the stiffnesses k_{em} and k_{wv} are considered in the state-space equations.

According to the non-clutch control strategy, the state variables x_s before clutch engaged stage are defined as

$$x_s = \Big[\theta_e - \theta_l - x_{1s}^{ref}\dot{\theta}_e - x_{2s}^{ref}\dot{\theta}_l - x_{3s}^{ref}T_{m1} - x_{4s}^{ref} \quad \theta_r - i_0\theta_f - x_{5s}^{ref}\dot{\theta}_r - x_{6s}^{ref}\dot{\theta}_f - x_{7s}^{ref}T_{m2} - x_{8s}^{ref}\Big]^T \tag{15}$$

where

$$\begin{aligned} x_{1s}^{ref} &= -J_e\ddot{\theta}_e/k_{em}, x_{2s}^{ref} = \omega_{ref}, x_{3s}^{ref} = \omega_{ref} \\ x_{4s}^{ref} &= (J_{M1} + J_e)\ddot{\theta}_l, x_{5s}^{ref} = J_v\ddot{\theta}_f + T_f/k_{wv} \\ x_{6s}^{ref} &= \omega_{ref}, x_{7s}^{ref} = \omega_{ref}/i_0 \\ x_{8s}^{ref} &= \left(J_{M2}\ddot{\theta}_r + J_v\ddot{\theta}_f + T_f\right)/i_0i_2 \end{aligned} \tag{16}$$

As the angles θ_e, θ_l, θ_r and θ_f are difficult to measure, the output state signals are defined as

$$y_s = \left[\dot{\theta}_l - x_{3s}^{ref}T_{m1} - x_{4s}^{ref}\dot{\theta}_r - x_{6s}^{ref}T_{m2} - x_{8s}^{ref}\right]^T \tag{17}$$

According to the performance indexes of MTP, the performance output signals can be defined as

$$z_s = \Big[\dot{\theta}_l - x_{2s}^{ref} \quad T_{m1} - x_{4s}^{ref} \quad \dot{\theta}_r - x_{6s}^{ref} \quad T_{m2} - x_{8s}^{ref} \quad \dot{T}_{m1} \quad \dot{T}_{m2} - u_{ss} \quad \dot{\theta}_r - i_0\dot{\theta}_f\Big]^T \tag{18}$$

Motor 1 is used to start the engine and engage the clutch, and motor 2 is used to meet the driver torque demand here. Thus, the control variables u_s are selected as

$$u_s = \left[\dot{T}_{m1} \quad \dot{T}_{m2} - u_{ss}\right]^T, u_{ss} = B_a\dot{x}_3^{ss}/(i_0i_2) \tag{19}$$

State-space equation of MTP system can be described as

$$\begin{cases} \dot{x}_s = A_sx + B_1^su + B_2^sw, w = \left[T_e \ \Delta B_a \ d\right]^T \\ y_s = C_y^sx, z_s = C_1^sx + D_1^su \end{cases} \tag{20}$$

In Stage 4, clutch is engaged. The state variables x_e, control variables u_e, and external inputs and disturbance w_e are defined as

$$\begin{aligned} x_e &= \Big[\theta_e - \theta_r - x_{1e}^{ref}\dot{\theta}_e - x_{2e}^{ref}\dot{\theta}_r - x_{3e}^{ref} \\ &\quad T_{m2} - x_{4e}^{ref}\theta_r - i_0\theta_f - x_{5e}^{ref}\dot{\theta}_f - x_{6e}^{ref}\Big] \\ u_e &= \dot{T}_{m2} - u^{ss}, w_e = \left[\Delta B_a \ d\right] \end{aligned} \tag{21}$$

where

$$\begin{aligned} x_{1e}^{ref} &= -\tfrac{J_{en}\ddot{\theta}_{en}}{k_{el}}, x_{2e}^{ref} = \omega_{ref}, x_{3e}^{ref} = \omega_{ref} \\ x_{4e}^{ref} &= \left(J_m\ddot{\theta}_r + J_v\ddot{\theta}_f + T_f\right)/i_0i_2 \\ x_{5e}^{ref} &= \left(J_v\ddot{\theta}_f + T_f\right)/k_{wv}, x_{6e}^{ref} = \omega_{ref}/i_0 \end{aligned} \tag{22}$$

Table 1 State matrix of mode transition system

$$A_1=\begin{bmatrix} 0 & 1 & -1 & 0 & 0 & 0 & 0 & 0 \\ -k_{em}/J_e & -C_{em}/J_e & C_{em}/J_e & 0 & 0 & 0 & 0 & 0 \\ k_{em}/J_{M1} & C_{el}/J_{M1} & -C_{em}/J_{M1} & 1/J_{M1} & 0 & 0 & 0 & 0 \\ 0 & 0 & 0 & 0 & 0 & 0 & 0 & 0 \\ 0 & 0 & 0 & 0 & 0 & 1/i_0 & -1 & 0 \\ 0 & 0 & 0 & 0 & -k_{wv}/J_{M2} & -C_{wv}/i_0J_{M2} & C_{wv}/J_{M2} & i_0i_2/J_{M2} \\ 0 & 0 & 0 & 0 & k_{wv}/J_v & C_{wv}/i_0J_v & -(C_{wv}+B_a)/J_v & 0 \\ 0 & 0 & 0 & 0 & 0 & 0 & 0 & 0 \end{bmatrix}$$

$$B_{11}=\begin{bmatrix} 0&0&0&1&0&0&0&0 \\ 0&0&0&0&0&0&0&1 \end{bmatrix}^T,\ B_{12}=\begin{bmatrix} 0&1/J_e&0&0&0&0&0&0 \\ 0&1&1&0&0&1&0&1 \\ 0&0&0&0&B_a\dot{\omega}_{ref}/(i_0k_{wv})&0&\Delta B_a/J_v&0 \end{bmatrix}^T$$

$$J_{M1}=J_{m1}+J_{cl},\ J_{M2}=\left(J_{m2}i_2{}^2+J_{cl}+J_{g1}+J_{g2}+J_{r1}+J_{r2}+J_{f1}\right)i_0+J_{f2}+J_w$$

$$A_2=\begin{bmatrix} 0 & 1 & -1 & 0 & 0 & 0 \\ -k_{em}/J_e & -C_{em}/J_e & C_{em}/J_e & 0 & 0 & 0 \\ i_0k_{em}/J_m & i_0C_{em}/J_m & -(i_0C_{em}+C_{wv}/i_0)/J_m & i_2/J_m & -k_{wv}/J_m & C_{wv}/J_m \\ 0 & 0 & 0 & 0 & 0 & 0 \\ 0 & 0 & 1 & 0 & 0 & -i_0 \\ 0 & 0 & C_{wv}i_0/J_v & 0 & k_{wv}i_0/J_v & -\left(C_{wv}i_0{}^2+B_a\right)/J_v \end{bmatrix}$$

$$B_{21}=\begin{bmatrix} 0&0&0&1&0&0 \end{bmatrix}^T,\ B_{22}=\begin{bmatrix} 0&0&0&0&B_a\dot{\omega}_{ref}/(i_0k_{wv})&1/J_{veh} \\ 0&1&1&1&0&0 \end{bmatrix}^T$$

$$J_m=J_{M2}+J_{M1}i_0$$

The output state signals are defined as

$$y_e=\begin{bmatrix}\dot{\theta}_r-x_{3e}^{ref} & T_{m2}-x_{4e}^{ref}\end{bmatrix}^T \tag{23}$$

The performance output signals

$$z_e=\begin{bmatrix}\dot{\theta}_r-x_{3e}^{ref} & T_{m2}-x_{4e}^{ref} & \dot{T}_{m2}-u_{ss} & \dot{\theta}_r-i_0\dot{\theta}_f\end{bmatrix}^T \tag{24}$$

Finally, the state-space equation can be described as

$$\begin{cases}\dot{x}_e=A_ex+B_1^eu+B_2^ew \\ y_e=C_y^ex,\ z_e=C_1^ex+D_1^eu\end{cases} \tag{25}$$

4.2 Modeling of random delays caused by CAN network

The effects of CAN-induced delays of control signals can be equivalent to the random real action time of control signals during one sampling period. Firstly, the continuous state-space equations of MTP without CAN-induced asynchronous random delays are discretized as

$$\begin{cases}x(k+1)=\hat{A}x_k+\hat{B}_1u_k+\hat{B}_2w_k,\ \hat{A}=e^{AT_s} \\ \hat{B}_1=\int_0^{T_s}e^{A(T_s-x)}B_1dx,\ \hat{B}_2=\int_0^{T_s}e^{A(T_s-x)}B_2dx\end{cases} \tag{26}$$

According to the difference of the transmitted control signals, the modeling of the random CAN-induced delay can be divided into two types. Model of type 1 assumes that the control signal is torque derivative, and model of type 2 assumes that the control signal is torque.

4.2.1 Asynchronous random delays modeling (transmitting torque derivative)

Considering the effects of delays, the discrete model of DM-PHEV system can be modified as [23]

$$\begin{aligned}x_{k+1}=&\hat{A}x_k+\hat{B}_1u_k+\hat{B}_2w_k+\Gamma_{0,k}(u_{k-1}-u_k)\\&+\Gamma_{1,k}(u_{k-2}-u_{k-1})+\ldots+\Gamma_{i,k}(u_{k-i-1}-u_{k-i})\end{aligned} \tag{27}$$

where

$$\Gamma_{i,k}=\begin{cases}0 & \tau_{k-i}-i\cdot T_s\le 0 \\ \int_0^{\tau_{k-i}-i\cdot T_s}e^{A(T_s-x)}B_1dx & 0\le\tau_{k-i}-i\cdot T_s\le T_s \\ \int_0^{T_s}e^{A(T_s-x)}B_1dx & \tau_{k-i}-i\cdot T_s\ge T_s\end{cases} \tag{28}$$

The random CAN-induced delays can be characterized by random system matrix $\Gamma_{i,k}$. The integral interval of matrix is the action time of control signal.

The upper bound of random CAN-induced delays is determined by the priority of CAN message, the length of frame and the transmission rate of CAN bus. The

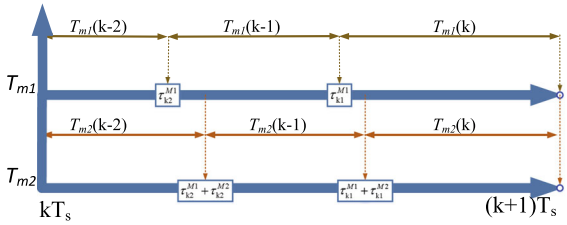

Fig. 6 Control signal delays of DM-PHEV

maximum delay of the ith priority CAN message $\tau_{\max,i}$ can be calculated as [27]

$$\tau_{\max,i} \le (j_i+2)l \Big/ \left(R_a - \sum_{j=0}^{i-1} \frac{l}{t_j} \right) \tag{29}$$

As stated in [28], $1.7T_s$ is a reasonable maximum CAN-induced delay in vehicle. T_s is the sampling period of control system. The CAN-induced delay is uniformly distributed in the interval $\left[0, \tau_{\max,i}\right]$ [29].

For DM-PHEV, dual motors have their own controllers, the control signals of two motors are transmitted in order according to the priority of message. So, the random delays for two motors are different as described in Fig. 6. The priority of CAN message of motor 1 is assumed as higher than that of motor 2. As shown in Fig. 6, the torque of motor 1 is delayed by τ_{ki}^{M1}, and the torque of motor 2 is delayed by τ_{ki}^{M2} on the basis of motor 1.

During one sampling period, the model of MTP with asynchronous random delays for two motors can be further transformed as

$$\begin{aligned} x(k+1) = {} & \hat{A}_1 x_k + \hat{B}_{11} u_k + \hat{B}_{12} w_k \\ & + \Gamma_{M1}^{k-1} B_{11}^{\tau} \left(\dot{T}_{m1}(k-1) - \dot{T}_{m1}(k) \right) \\ & + \Gamma_{M1}^{k-2} B_{11}^{\tau} \left(\dot{T}_{m1}(k-2) - \dot{T}_{m1}(k-1) \right) \\ & + \Gamma_{M2}^{k-1} B_{12}^{\tau} \left(T_{m2}(k-1) - T_{m2}(k) \right) \\ & + \Gamma_{M2}^{k-2} B_{12}^{\tau} \left(T_{m2}(k-2) - T_{m2}(k-1) \right) \end{aligned} \tag{30}$$

where

$$\begin{cases} \Gamma_{M1}^{k-1} = \Gamma_{k1}^{M1},\ \Gamma_{M2}^{k-1} = \Gamma_{k1}^{M1} + \Gamma_{k1}^{M2} \\ \Gamma_{M1}^{k-2} = \Gamma_{k2}^{M1},\ \Gamma_{M2}^{k-2} = \Gamma_{k2}^{M1} + \Gamma_{k2}^{M2} \\ B_{11}^{\tau} = \left[0\ 0\ 0\ 1\ 0\ 0\ 0\ 0 \right]^T \\ B_{12}^{\tau} = \left[0\ 0\ 0\ 0\ 0\ 0\ 0\ 1 \right]^T \end{cases} \tag{31}$$

Similar to Eq.(28), the coefficient of control signals can be described as

$$\begin{cases} \Gamma_{k2}^{M1} = \int_0^{\tau_{k2}^{M1}} e^{A(T_s - x)} dx,\ \tau_{k2}^{M1} \in [0, 0.7T_s] \\ \Gamma_{k1}^{M1} = \int_0^{\tau_{k1}^{M1}} e^{A(T_s - x)} dx,\ \tau_{k1}^{M1} \in [0, T_s] \\ \Gamma_{k1,2}^{M2} = \int_0^{\tau_{k1,2}^{M2}} e^{A(T_s - x)} dx,\ \tau_{k1,2}^{M2} \in [0, 0.2T_s] \end{cases} \tag{32}$$

It is assumed that the delay of the motor 2 relative to the motor 1 is less than 0.2 T_s.

The nonlinearity of the model with ACDs makes it difficult to design a coordinated controller, so the model needs to be linearized.

According to Taylor series expansion, the random delay time Γ_{k2}^{M1} can be linearized as [30]

$$\begin{aligned} \Gamma_{k2}^{M1}(x) &= \Gamma(0) + \dot{\Gamma}(0)x + \cdots + \frac{d^n \Gamma(0)}{dx^n} \frac{x^n}{n!} + \cdots \\ &\approx -\sum_{i=1}^{j} \frac{(-x)^i}{i!} A^{i-1} e^{AT s} \end{aligned} \tag{33}$$

Furthermore, Eq.(33) can be rewritten as

$$\begin{cases} \Gamma_{k2}^{M1}(x) = A_\Gamma x_\Gamma \ \ x_\Gamma \in [x_{\min}, x_{\max}] \\ A_\Gamma = \left[\frac{(-1)^2}{1!} A^0 e^{AT_s} \ \cdots \ \frac{(-1)^{i+1}}{i!} A^{i-1} e^{AT_s} \right] \\ x_\Gamma = \left[x \ \cdots \ x^i \right]^T \end{cases} \tag{34}$$

According to [30,31], convex polytope is adopted here to describe the uncertainties of delays.

Define $x_{\Gamma,i}$ as

$$\begin{aligned} & x_{\tau,0} = \left[x_{\min}\ x_{\min}^2 \cdots x_{\min}^i \right]^T \\ & x_{\tau,1} = \left[x_{\max}\ x_{\min}^2 \cdots x_{\min}^i \right]^T \\ & \vdots \\ & x_{\tau,i+1} = \left[x_{\max}\ x_{\max}^2 \cdots x_{\max}^i \right]^T \end{aligned} \tag{35}$$

Replacing x_Γ in Eq.(34) with

$$x_\Gamma = \sum_{i=1}^{j+1} \lambda_i(k) x_{\tau,i},\ \lambda_i(k) > 0,\ \sum_{i=1}^{j+1} \lambda_i(k) = 1 \tag{36}$$

$\Gamma(x)$ in Eq.(34) can be represented as

$$\Gamma(x) = \sum_{i=1}^{j+1} A_\Gamma \lambda_i(k) x_{\Gamma,i} \tag{37}$$

After the linearization of nonlinear terms, new states space equations are defined as

$$\begin{cases} \tilde{x}(k+1) = \tilde{A}_1 \tilde{x}(k) + \tilde{B}_{11} u(k) + \tilde{B}_{12} w(k) \\ \tilde{y} = \tilde{C}_y \tilde{x},\ \tilde{z} = \tilde{C}_1 \tilde{x} + \tilde{D}_1 u \\ \tilde{x} = \left[x\ \bar{T} \right]^T,\ \tilde{y} = \left[y\ \bar{T} \right]^T,\ \tilde{z} = \left[z\ \bar{T} \right]^T \end{cases} \tag{38}$$

where

$$\bar{T}=\left[\dot{T}_{m1}(k-1)\ \dot{T}_{m2}(k-1)\ \dot{T}_{m1}(k-2)\ \dot{T}_{m2}(k-2)\right]$$

$$\tilde{A}_1=\begin{bmatrix}\hat{A}_1 & \Gamma_\tau^1 & \Gamma_\tau^2 & \Gamma_{M1}^{k-2}B_{11}^\tau & \Gamma_{M2}^{k-2}B_{12}^\tau\\ \mathbf{0} & 0 & 0 & 0 & 0\\ \mathbf{0} & 0 & 0 & 0 & 0\\ \mathbf{0} & 1 & 0 & 0 & 0\\ \mathbf{0} & 0 & 1 & 0 & 0\end{bmatrix}$$

$$\tilde{B}_{11}=\left[B_{1d}^l-\Gamma_{M1}^{k-1}B_{11}^\tau-\Gamma_{M2}^{k-1}B_{12}^\tau\ B_\kappa^1\ B_\kappa^2\ \mathbf{0}\ \mathbf{0}\right]^T$$

$$B_\kappa^1=\left[1\ 0\right]^T,\ B_\kappa^2=\left[0\ 1\right]^T,\ \tilde{B}_{12}=\begin{bmatrix}\hat{B}_{12} & \mathbf{0}\end{bmatrix}^T$$

$$\Gamma_\tau^1=\Gamma_{M1}^{k-1}B_{11}^\tau-\Gamma_{M1}^{k-2}B_{11}^\tau,$$

$$\Gamma_\tau^2=\Delta_{M2}^{k-1}B_{12}^\tau-\Gamma_{M2}^{k-2}B_{12}^\tau \tag{39}$$

4.2.2 Asynchronous random delays modeling (transmitting torque)

If the control signal transmitted by CAN is the torque of actuators, Eq.(27) can be further transformed as Eq.(40).

$$\begin{aligned}x(k+1)=&A_d^l x(k)+B_{1d}^l u(k)+B_{2d}^l w(k)\\&+\Gamma_{M1}^{k-1}B_{11}^\tau\left(T_{m1}(k-1)-T_{m1}(k)\right)\\&+\Gamma_{M1}^{k-2}B_{11}^\tau\left(T_{m1}(k-2)-T_{m1}(k-1)\right)\\&+\Gamma_{M2}^{k-1}(k)B_{12}^\tau\left(T_{m2}(k-1)-T_{m2}(k)\right)\\&+\Gamma_{M2}^{k-2}(k)B_{12}^\tau\left(T_{m2}(k-2)-T_{m2}(k-1)\right)\end{aligned} \tag{40}$$

where

$$\begin{cases}B_{11}^\tau=\left[0\ 0\ 1/J_{M1}\ 0\ 0\ 0\ 0\ 0\right]^T\\ B_{12}^\tau=\left[0\ 0\ 0\ 0\ 0\ i_2/J_{M2}\ 0\ 0\right]^T\end{cases} \tag{41}$$

Similar to the derivative torque transmitted by CAN, new state variables can be defined as

$$\begin{aligned}\tilde{x}(k)=&\left[x(k)\ T_{m1}(k-1)\ T_{m2}(k-1)\right.\\&\left.T_{m1}(k-2)\ T_{m2}(k-2)\right]^T\end{aligned} \tag{42}$$

Then, the new state-space equation can be rewritten as

$$\tilde{A}_1=\begin{bmatrix}\hat{A}_1-\Gamma_\tau^1 & \Gamma_\tau^2 & \Gamma_{M1}^{k-2}B_{11}^\tau & \Gamma_\tau^3 & \Gamma_{M2}^{k-2}B_{12}^\tau\\ \kappa_1 & 0 & 0 & 0 & 0\\ \kappa_2 & 0 & 0 & 0 & 0\\ 0 & 1 & 0 & 0 & 0\\ 0 & 0 & 1 & 0 & 0\end{bmatrix} \tag{43}$$

$$\tilde{B}_{11}=\begin{bmatrix}\hat{B}_{11} & \mathbf{0}\end{bmatrix},\ \tilde{B}_{12}=\begin{bmatrix}\hat{B}_{12} & \mathbf{0}\end{bmatrix}$$

where

$$\begin{cases}\kappa_1=\left[0\ 0\ 0\ 1\ 0\ 0\ 0\ 0\right]^T\\ \kappa_2=\left[0\ 0\ 0\ 0\ 0\ 0\ 0\ 1\right]^T\\ \Gamma_\tau^1=\Gamma_{M1}^{k-1}B_{11}^{\tau T}\kappa_1+\Gamma_{M2}^{k-1}B_{12}^{\tau T}\kappa_2\\ \Gamma_\tau^2=\Gamma_{M1}^{k-1}B_{11}^\tau-\Gamma_{M1}^{k-2}B_{11}^\tau\\ \Gamma_\tau^3=\Gamma_{M2}^{k-1}B_{12}^\tau-\Gamma_{M2}^{k-2}B_{12}^\tau\end{cases} \tag{44}$$

The model of other stages can be acquired by the same way, so other state-space equations are omitted.

4.3 Output feedback H_∞ coordinated controller

The goal of coordinated controller is to design a control law $u=\tilde{K}y$ such that the MTP system is asymptotically stable and the H_∞ norm from w to z is less than γ_∞.

$$\sup_{w\neq 0}\|z\|_2<\gamma_\infty\|w\|_2 \tag{45}$$

According to [32], the MTP system is asymptotically stable and the H_∞ norm is less than γ_∞ if there exists a Lyapunov function $V(x(k))=x^TPx$, $P=P^T>0$ such that

$$\begin{aligned}&V(x(k+1))-V(x(k))\\&+\left\|\hat{z}_2(k)\right\|_2-{\gamma_\infty}^2\|w(k)\|_2<0\end{aligned} \tag{46}$$

For MTP system, Eq. (46) can be written as the following inequality

$$\begin{aligned}&\left[\tilde{A}_\chi x(k)+B_2^\chi w(k)\right]^T P\,[*]-x(k)^TP\,[*]\\&+\left[\tilde{C}_1^\chi x(k)\right]^T[*]-{\gamma_\infty}^2w(k)^T[*]<0\end{aligned} \tag{47}$$

Inequality Eq.(47) can be rewritten in the following matrix:

$$\begin{bmatrix}x\\ w\end{bmatrix}^T\Omega\begin{bmatrix}x\\ w\end{bmatrix}<0 \tag{48}$$

where

$$\Omega=\begin{bmatrix}\tilde{C}_1\\ \mathbf{0}\end{bmatrix}(*)+\begin{bmatrix}\tilde{A}\\ \tilde{B}_2\end{bmatrix}P\,(*)+\begin{bmatrix}-P & 0\\ 0 & -{\gamma_\infty}^2I\end{bmatrix} \tag{49}$$

Further, by using Schur complement for Eq.(49), following inequality can be derived.

$$\begin{bmatrix}-P & \tilde{C}_1 & 0 & \tilde{A}\\ 0 & -I & 0 & 0\\ 0 & 0 & -{\gamma_\infty}^2I & \tilde{B}_2\\ 0 & 0 & 0 & -P^{-1}\end{bmatrix}<0 \tag{50}$$

Pre- and post-multiplying Eq.(50) by

$$\mu=\mathrm{diag}\left\{P^{-1}\ I\ I\ I\right\} \tag{51}$$

and μ^T, respectively, and then applying $P=P^{-1}$, $KP=W$, we can obtain that

$$\begin{bmatrix}-P & \mathbf{0} & \tilde{A}P+\tilde{B}_1W & \tilde{B}_2\\ * & -\gamma_\infty I & \tilde{C}_1P+\tilde{D}_1W & \mathbf{0}\\ * & * & -P & \mathbf{0}\\ * & * & * & -\gamma_\infty I\end{bmatrix}<0 \tag{52}$$

Pre- and post-multiplying Eq.(50) by ${\sigma_{1,2}}^{\mathrm{T}}$ and $\sigma_{1,2}$, respectively.

$$ {\sigma_1}^{\mathrm{T}} = \mathrm{diag}\left\{ I \;\; P^{-1}G \right\}, {\sigma_2}^{\mathrm{T}} = \mathrm{diag}\left\{ I \;\; P^{-1}G \;\; I \right\} \quad (53) $$

Due to that $P - G - G^T \geq -G^T P^{-1} G$ [33], and applying $Y = KG$ we can obtain that

$$ \begin{bmatrix} P - G - G^T & \mathbf{0} & \tilde{A}G + \tilde{B}_1 Y & \tilde{B}_2 \\ * & -I & \tilde{C}_1 G + \tilde{D}_1 Y & \mathbf{0} \\ * & * & -P & \mathbf{0} \\ * & * & * & -{\gamma_\infty}^2 I \end{bmatrix} < 0 \quad (54) $$

Finally, the desired state-feedback gain K can be calculated in MATLAB by using LMI toolbox as

$$ K = YG^{-1} \quad (55) $$

According to [34–36], the output feedback controller can be derived from the state feedback controller as

$$ u = YG^{-1}x = \tilde{K}y = \tilde{K}\tilde{C}_y x \quad (56) $$

Defining $G_Q = {G_Q}^T$, $G_R = {G_R}^T$, Y_R, R, Q and substituting Y and G in Eq.(55) with G_Q, G_R and Y_R as

$$ G = QG_Q Q^T + RG_R R^T, Y = Y_R R^T \quad (57) $$

where

$$ \begin{cases} Q = null\left(\tilde{C}_y\right), R = \tilde{C}_y^{\dagger} + QL, \tilde{C}_y^{\dagger} = \tilde{C}_y^T \left(\tilde{C}_y \tilde{C}_y^T\right)^{-1} \\ L = Q^{\dagger} G \tilde{C}_y^T (\tilde{C}_y G \tilde{C}_y^T)^{-1}, Q^{\dagger} = \left(Q^T Q\right)^{-1} Q^T \end{cases} \quad (58) $$

Finally, the desired output-feedback gain $\tilde{K}$ can be calculated as [34]

$$ \tilde{K} = Y_R {G_R}^{-1} \quad (59) $$

5 Simulation and HiL test results

To verify the effectiveness of RCAT and RCAD non-clutch coordinated controllers, simulation and HiL tests are conducted in this section. The simulation model of MTP system is developed in MATLAB/Simulink. CAN environment model for the communication between controller and MTP system is developed in MATLAB/SimEvent. The model of ACDs is realized by the random number of messages transmitted by CAN. And the transmission order is set to simulate the different priorities of CAN messages. For comparison, a traditional robust H_∞ coordinated controller (RHCC) without considering CAN-induced delays is also applied to the MTP system. RHCC is designed based on model in Eq.(25) according to the method provided in [32]. The output feedback gains of MTP can be gotten as

$$ \begin{aligned} K_s &= \begin{bmatrix} -152.96 & -21.12 & 0 & 0 \\ 0 & 0 & -150.71 & -12.10 \end{bmatrix} \\ K_e &= [-80.25 \;\; -5.84] \end{aligned} \quad (60) $$

The output feedback gains of RCAT can be gotten as

$$ \begin{aligned} K_s &= \begin{bmatrix} K_s^1 & K_s^2 \end{bmatrix} \\ K_s^1 &= \begin{bmatrix} -44.45 & -19.49 & 0 & 0 \\ 0 & 0 & -34.84 & -11.38 \end{bmatrix} \\ K_s^1 &= \begin{bmatrix} 1.81 & 0 & -4.03 & 0 \\ 0 & -10.41 & 0 & -1.04 \end{bmatrix} \\ K_e &= \begin{bmatrix} -72.49 & -4.97 & 1.01 & -0.73 \end{bmatrix} \end{aligned} \quad (61) $$

The output feedback gains of RCAD can be gotten as

$$ \begin{aligned} K_s &= \begin{bmatrix} K_s^1 & K_s^2 \end{bmatrix} \\ K_s^1 &= \begin{bmatrix} -72.17 & -31.94 & 0 & 0 \\ 0 & 0 & -31.28 & -7.94 \end{bmatrix} \\ K_s^1 &= \begin{bmatrix} -0.34 & 0 & -0.18 & 0 \\ 0 & -0.16 & 0 & -0.21 \end{bmatrix} \\ K_e &= \begin{bmatrix} -11.00 & -0.70 & 0.60 & 0.08 \end{bmatrix} \end{aligned} \quad (62) $$

An acceleration condition is used to verify the effect of the proposed control strategy. The reference speed of clutch disks can be calculated according to the reference speed of vehicle as

$$ \omega_{ref} = v_{ref} / R_t \quad (63) $$

5.1 Simulation and results analysis

5.1.1 MTP results analysis without delays

Firstly, the MTP system under ideal network is simulated as shown in Fig. 7. The changes of stage for MTP system under different controllers are shown in Fig. 7a. It can be seen that the time of MTP controlled by RHCC is minimum, which is about 0.6 s. The time of MTP controlled by RCAT is maximum, which is about 1.4 s. Correspondingly, the maximum vehicle jerk of MTP controlled by RHCC is about 4 $\mathrm{m/s^3}$ as shown in Fig. 7b, which is obviously greater than that controlled by RCAT and RCAD. Because RCAT and RCAD consider the influence of possible network-induced delays, the corresponding control laws are more conservative

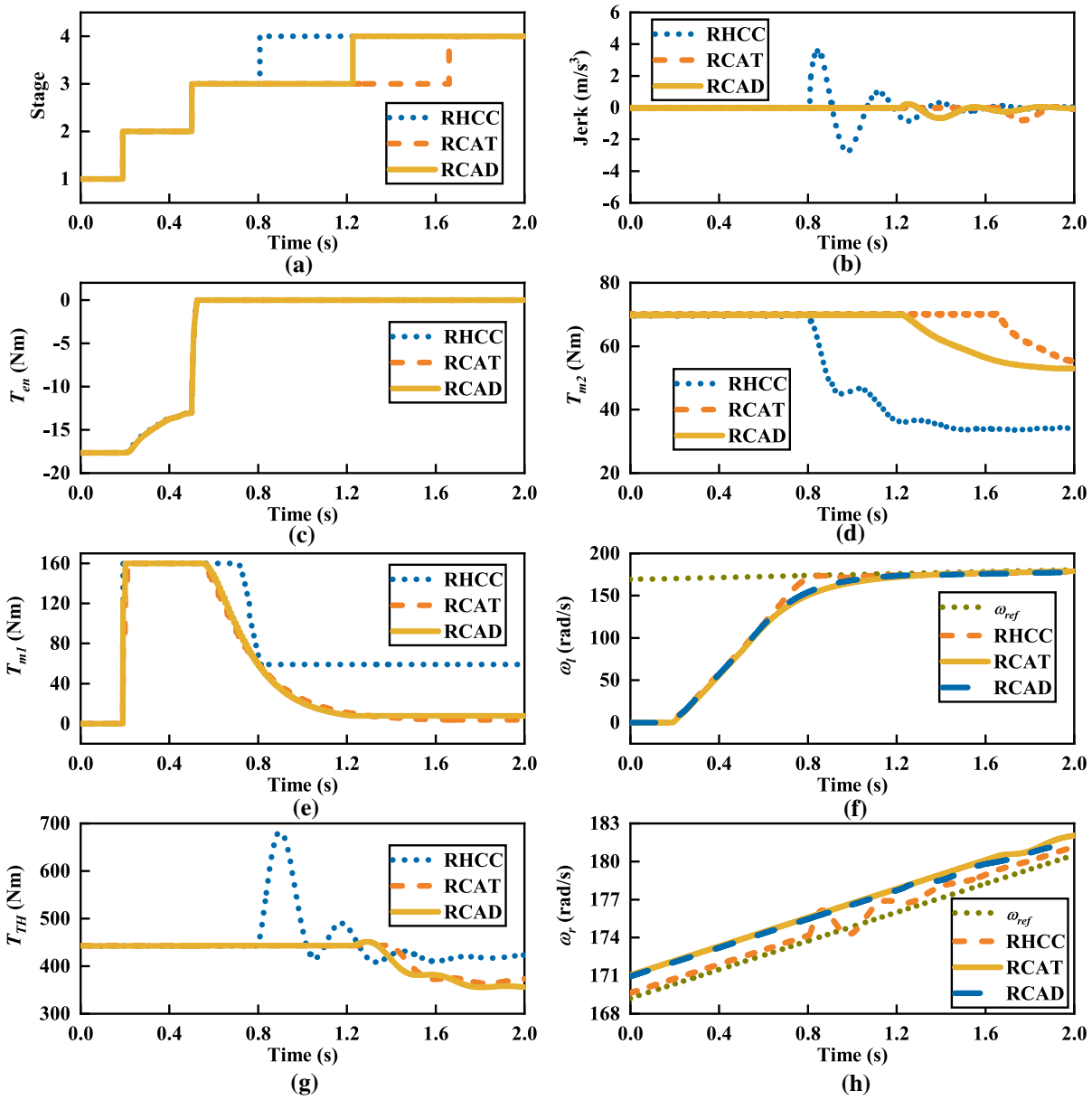

Fig. 7 Results of MTP without delays. **a** Stage of MTP. **b** Vehicle jerk. **c** Torque of engine. **d** Torque of motor 2. **e** Torque of motor 1. **f** Comparison of actual ω_l and reference ω_{ref}. **g** Torque transmitted to tire. **h** Comparison of actual ω_r and reference ω_{ref}

than RHCC. Under these two controllers, the vehicle jerk is smaller, but the time of MTP is correspondingly increased. Figure 7c is the torque of engine. The engine is worked as the load of the motor 1 in Stage 2, and the motor 1 overcomes the resistance torque of the engine to start the engine. So, the torque of engine in Stage 2 is resistance torque. In order to avoid the vehicle jerk caused by the ripple torque of the engine, the engine torque will keep zero temporarily after the engine is started. Figure 7d is the torque of motor 2 which works as the compensated torque to keep the speed of vehicle stable. Figure 7e is the torque of motor 1 which works to start the engine and accelerates the clutch-driven disk to engage the clutch C2. It can be seen that the torque of motor 1 decreased in the end of Stage 3 to smoothly engage the clutch. Smaller torque of motor

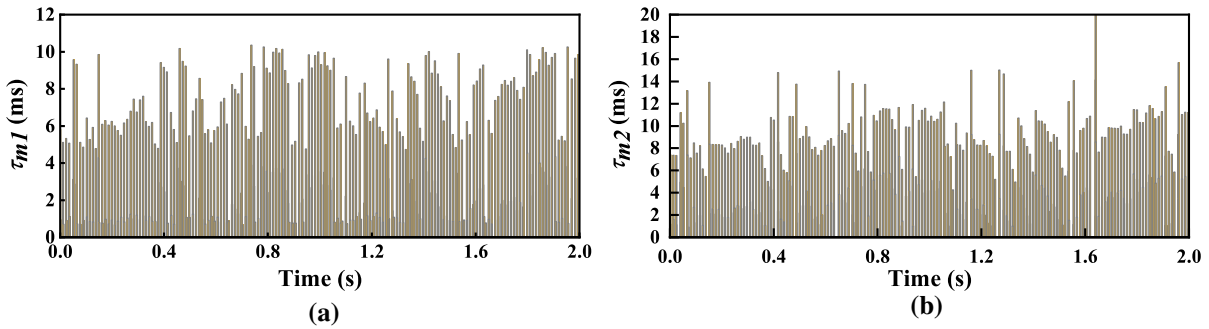

Fig. 8 CAN network-induced time delays. **a** Time delay of motor 1. **b** Time delay of motor 2

1 in the end of stage 3 leads to smaller vehicle jerk, which can be verified in Fig. 7b. The speeds of clutch-driven and driving disk are shown in Fig. 7f and h, respectively. The speed of clutch driven disk ω_l rises quickly at first, and then, it tracks the reference speed smoothly. The speed of clutch-driven disk ω_r is also controlled to track the reference speed. It can be seen from Fig. 7h that the tracking error under RHCC controller is the smallest, but there are large fluctuations when clutch engaged, while the tracking errors under RCAT and RCAD which take into account the effects of CAN-induced delays are larger, but the fluctuations of speed are small. The torque transmitted to the tire T_{TH} is shown in Fig. 7g. It can be seen that the fluctuation of T_{TH} controlled by RHCC is much bigger than that controlled by others, which is also consistent with the results in Fig. 7b. In conclusion, both the RHCC, RCAT and RCAD can work well for the mode transition process without CAN-induced delays.

5.1.2 MTP results analysis with ACDs

The sampling period of controllers is 0.01 s, so the maximum value of ACDs is set as 17 ms. The random time delays set in the simulation for each actuators are given in Fig. 8. As modeled before, the CAN-induced delay for actuator is consistent with the priority of its communication node. It can be seen that the maximum delay for motor 2 is within 17 ms.

To compare the performance of coordinated controllers under ACDs which shown in Fig. 8, simulations of MTP with ACDs are conducted and the results are shown in Fig. 9. It can be seen that the performance of proposed RCAT and RCAD are obviously better than that of RHCC. The vehicle jerk controlled by RCAT is bigger than that shown in Fig. 7b, but it is much smaller than the maximum vehicle jerk controlled by RHCC which is closed to 11 m/s^3. The shock is mainly caused by the ACDs which results in the large torque of motor 1 in the end of Stage 3. The vehicle jerk is also reflected in the fluctuation of the speed of the clutch driving disk. The tracking errors of RCAT and RCAD are also reduced under MTP with CAN-induced delays. And the tracking error of RHCC is larger than those of other controllers. So, for MTP with CAN-induced delays, RCAT and RCAD controllers are necessary.

To further organize the improvements, the comparison table is given. Table 2 denotes the jerk, MTP time and the value of errors between the indexes of RCAT, RCAD and RHCC works on MTP with ACDs. As represented in table, both the RCAT and RCAD improved the vehicle jerk, but they cost a little longer time for MTP than RHCC.

5.2 HiL test and results analysis

The calculation speed of coordinated controller in simulation can be assumed as instantaneous. However, the performance of actual controller is limited. Thus, the simulation only verifies the effectiveness of proposed controllers theoretically. As for the actual vehicle experiment, the cost is high and the safety of the controller strategy directly applied to the vehicle cannot be guaranteed. Thus, a HiL test with actual controller, virtual DM-PHEV and virtual CAN bus is a good choice to verify the real-time performance of RCAT and RCAD. As shown in Fig. 10, the control strategy based on the MotoHawk module library is compiled and downloaded into the rapid prototype controller. The plant model of DM-PHEV is built in NI system and downloaded into the NI real-time simulator to simulate the

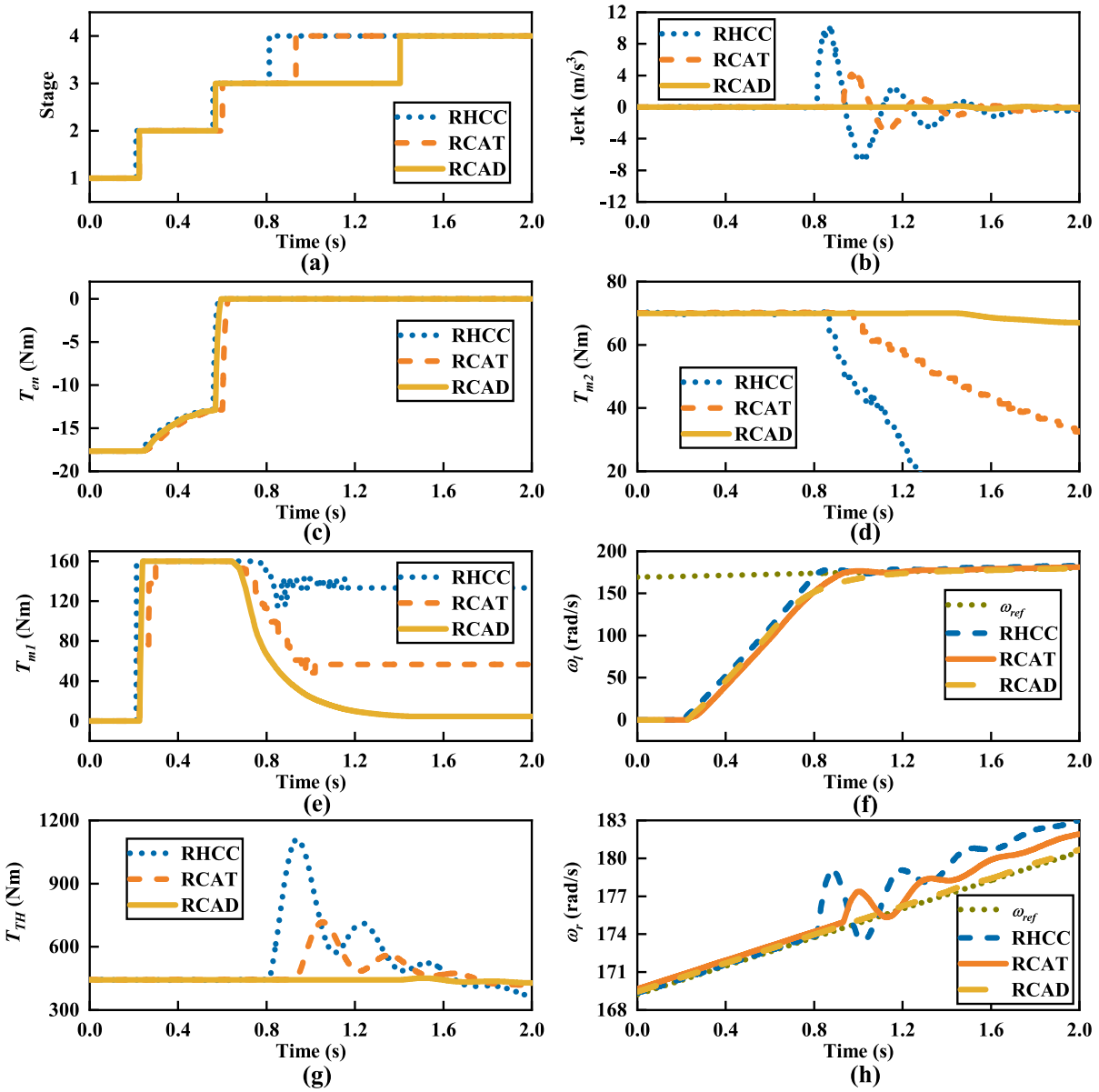

Fig. 9 Results of MTP with delays. **a** Stage of MTP. **b** Vehicle jerk. **c** Torque of engine. **d** Torque of motor 2. **e** Torque of motor 1. **f** Comparison of actual ω_l and reference ω_{ref}. **g** Torque transmitted to tire. **h** Comparison of actual ω_r and reference ω_{ref}

Table 2 Quantitative comparison results of simulation

	RHCC	RCAT	RCAD
Jerk(m/s^3)	10.3	4.3	0.2
Time(s)	0.6	0.7	1.2
Deviation of jerk	x	58.3%	98.1%
Deviation of time	x	-16.67%	-100%

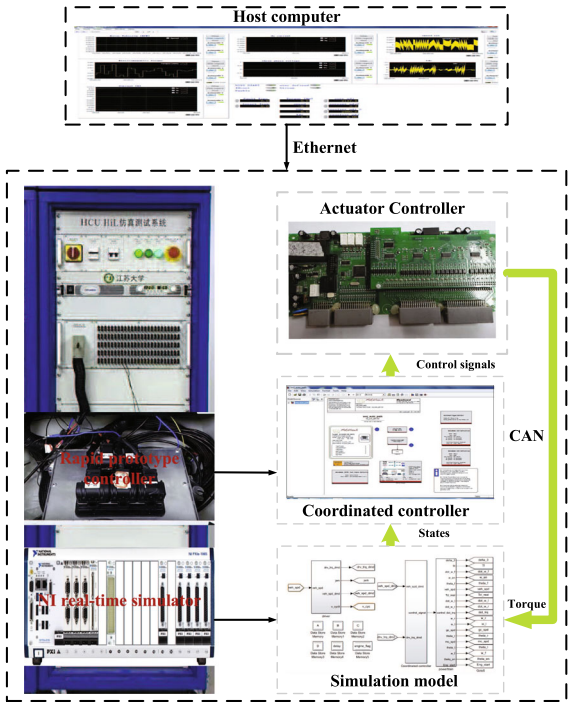

Fig. 10 Schematic diagram of HiL test

operation of PHEV. The communication between NI real-time simulator and rapid prototype controller is through CAN bus. Besides, micro-controller unit is adopted as the actuator controller. The operation of HiL system can be controlled by the host computer. To simulate the CAN-induced delays, the actuator controller is inserted in the CAN communication system and it can receive the information from rapid prototype controller and NI real-time simulator. Then, it will hold the information for a random time which is less than 1.7 T_s to simulate the random CAN-induced delays.

The test results of MTP without simulated CAN-induced delays are shown in Fig. 11. And the comparisons between RCAT and RCAD are shown in Fig. 12. The test results are similar to the simulation results. Because of the noise of information transmission between controller and NI real-time simulator and the limitation of controller operation accuracy and speed, the results are a little worse than simulation, but the trend is similar. The HiL results of MTP with simulated ACDs controlled by three controllers once again confirm the necessity of considering the influence of ACDs to design the coordinated controller. As shown in Fig. 12b, the vehicle jerk controlled by RHCC is much bigger than those controlled by the others. And at the end of clutch slipping stage, the maximum vehicle jerk of RHCC reached approximately 11 m/s^3, which will damage the driving comfort. The ride comfort performance of MTP controlled by RCAT and RCAD is much better than that controlled by RHCC. However, the time of MTP controlled by RCAD is longer than MTP controlled by RCAT and RHCC, which is consistent with the results in simulation. Economy performance is sacrificed for better driving comfort. The quantitative results of MTP with ACDs are shown in Table 3. Compared with the traditional RHCC controller, the vehicle jerk of DM-PHEV with ACDs can be reduced by 52.6% and 96.66% via the proposed RCAT and RCAD controller, respectively. The mode transition time of RCAT and RCAD is increased by 12.31% and 61.54%, respectively. The little scarification of mode transition time can improve the ride comfort of passengers. In short, the HiL test results verify the effectiveness of proposed coordinated control strategy. Although the RCAD controller can acquire minimal vehicle jerk, the mode switching time for MTP with random ACDs is much longer than that controlled by RCAT. Longer transition time is not conducive to improving fuel economy. Thus, RCAT controller effectively reduces the vehicle jerk without too much extension of mode transition time.

6 Conclusion

In this paper, a smooth MTP without clutch slipping stage can be achieved by the proposed non-clutch coordinated control strategy. Moreover, for DM-PHEV control system with ACDs, RCAT and RCAD coordinated controllers considering CAN-induced asynchronous random delays in MTP are proposed. The main conclusions are shown the following:

(1) ACDs exists in MTP system result in the uncoordinated torque of actuators and traditional RHCC controller cannot effectively reduce the vehicle jerk.
(2) Compared with RHCC, the vehicle jerk of MTP system under RCAT and RCAD control is reduced by 52.6 % and 96.66 %, respectively.
(3) Although the RCAD controller can obtain minimal vehicle jerk, the mode switching time is greatly increased, which is not conducive to improving fuel economy.

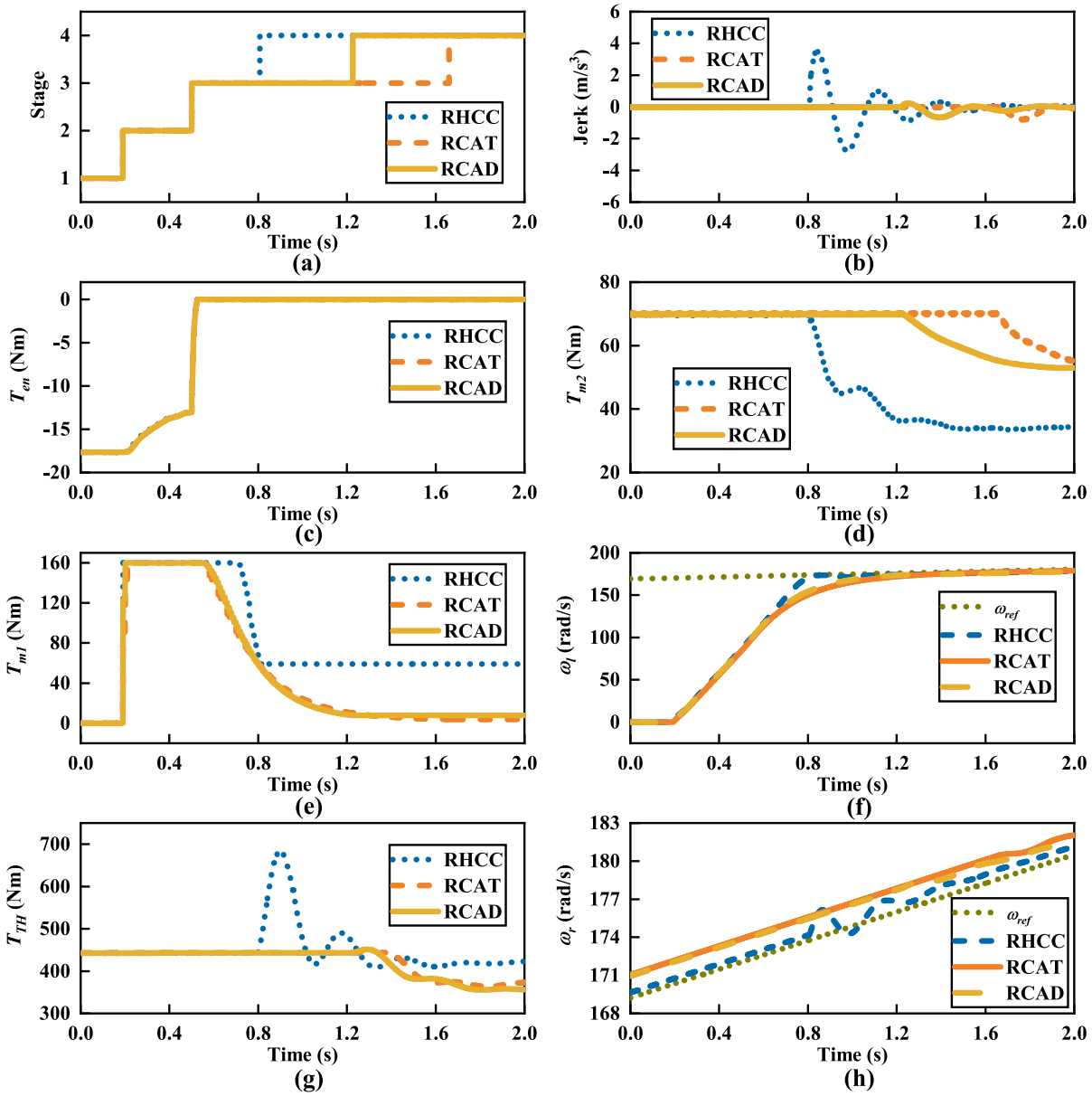

Fig. 11 HiL results without delays. **a** Stage of MTP. **b** Vehicle jerk. **c** Torque of engine. **d** Torque of motor 2. **e** Torque of motor 1. **f** Comparison of actual ω_l and reference ω_{ref}. **g** Torque transmitted to tire. **h** Comparison of actual ω_r and reference ω_{ref}

Table 3 Quantitative comparison results of HiL

	RHCC	RCAT	RCAD
Jerk (m/s^3)	10.77	5.1	0.36
Time (s)	0.65	0.73	1.05
Deviation of jerk	x	52.6%	96.66%
Deviation of time	x	−12.31%	−61.54%

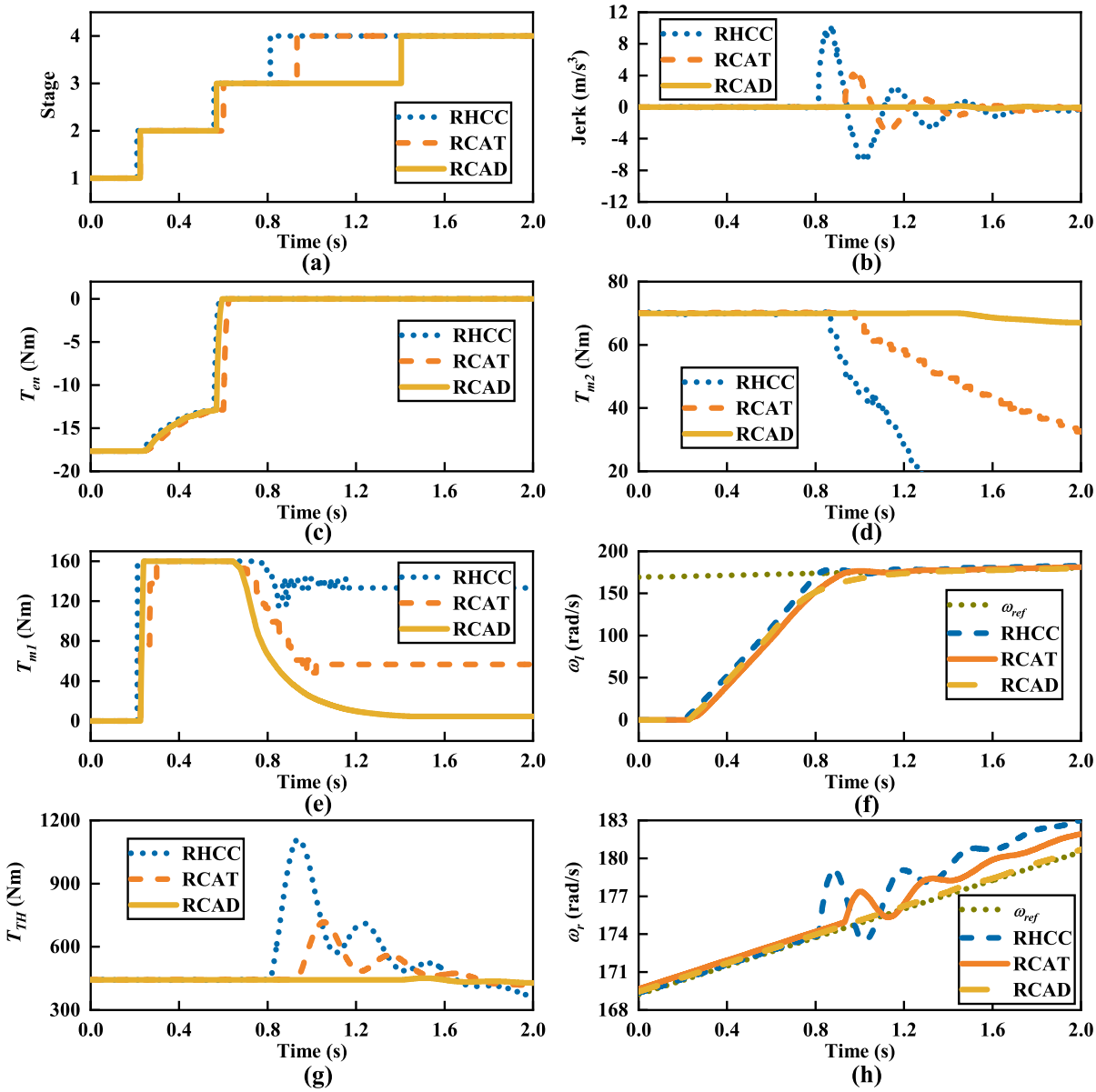

Fig. 12 HiL results with delays. **a** Stage of MTP. **b** Vehicle jerk. **c** Torque of engine. **d** Torque of motor 2. **e** Torque of motor 1. **f** Comparison of actual ω_l and reference ω_{ref}. **g** Torque transmitted to tire. **h** Comparison of actual ω_r and reference ω_{ref}

(4) RCAT controller can simultaneously obtain acceptable jerk and shorter mode switching time.

In conclusion, for the pursuit of extreme ride comfort scenarios, RCAD controller is a better choice. RCAT coordinates the performance of comfort and economy, and can be more widely used. In the future, the dynamic characteristics of motors will be introduced to improve the design of the controller.

Acknowledgements This work is financially supported by the National Key Research and Development Project [No. 2017YFB0103200], Graduate Research and Innovation Projects of Jiangsu Province [KYCX21_3330], the National Natural Science Foundation of China [No. 51705204], Six Talent Peaks Project in Jiangsu Province (CN) [No. JXQC-036], the China Scholarship Council [No. 202008690006, No. 201908320221].

Data availability The datasets generated during and/or analyzed during the current study are available from the corresponding author on reasonable request.

Declarations

Conflict of interest The authors declare that they have no conflict of interest.

References

1. Zhang, H., Qin, Y., Li, X., Liu, X., Yan, J.: Power management optimization in plug-in hybrid electric vehicles subject to uncertain driving cycles. eTransportation **3**, 100029 (2020)
2. Kim, S., Choi, S.B.: Cooperative control of drive motor and clutch for gear shift of hybrid electric vehicles with dual-clutch transmission. IEEE/ASME Trans. Mechatron. **25**(3), 1578–1588 (2020)
3. Chen, B., Evangelou, S.A., Lot, R.: Series hybrid electric vehicle simultaneous energy management and driving speed optimization. IEEE/ASME Trans. Mechatron. **24**(6), 2756–2767 (2019)
4. Liu, Y., Chen, D., Lei, Z., Qin, D., Zhang, Y., Wu, R., Luo, Y.: Modeling and control of engine starting for a full hybrid electric vehicle based on system dynamic characteristics. Int. J. Autom. Technol. **18**, 911–922 (2017)
5. Su, Y., Hu, M., Su, L., Qin, D., Zhang, T., Fu, C.: Dynamic coordinated control during mode transition process for a compound power-split hybrid electric vehicle. Mech. Syst. Signal Process. **107**, 221–240 (2018)
6. Song, S., Guan, Y., Fu, Z., Li, H.: Switching control from motor driving mode to hybrid driving mode for phev. In: 2017 Chinese Automation Congress (CAC), pp. 4209–4214 (2017)
7. Shen, D., Guehmann, C., Zhang, T.: Coordinated mode transition control for a novel compound power-split hybrid electric vehicle. In: WCX SAE World Congress Experience (2019)
8. Li, K., Sun, J., Liu, X., Zhang, C.: Torque coordinated control of phev based on the fuzzy and sliding mode method with load torque observer. In: Proceedings of the 33rd Chinese Control Conference, pp. 7933–7937 (2014)
9. Fu, Z., Su, P., Song, S., Tao, F.: Mode transition coordination control for phev based on cascade predictive method. IEEE Access **7**, 138403–138414 (2019)
10. Tang, X., Yang, K., Liu, T., Qin, Y., Zhang, D., Ji, Q.: Transient dynamic response analysis of engine start for a hybrid electric vehicle. In: 2019 3rd Conference on Vehicle Control and Intelligence (CVCI), pp. 1–6 (2019)
11. Zeng, X., Yang, N., Wang, J., Song, D., Zhang, N., Shang, M., Liu, J.: Predictive-model-based dynamic coordination control strategy for power-split hybrid electric bus. Mech. Syst. Signal Process. **60–61**, 785–798 (2015)
12. Wang, C., Zhao, Z., Zhang, T., Li, M.: Mode transition coordinated control for a compound power-split hybrid car. Mech. Syst. Signal Process. **87**, 192–205 (2017)
13. Yang, C., Shi, Y., Li, L., Wang, X.: Efficient mode transition control for parallel hybrid electric vehicle with adaptive dual-loop control framework. IEEE Trans. Vehic. Technol. **69**(2), 1519–1532 (2020)
14. Chen, L., Xi, G., Sun, J.: Torque coordination control during mode transition for a series-parallel hybrid electric vehicle. IEEE Trans. Vehic. Technol. **61**(7), 2936–2949 (2012)
15. Xu, X., Liang, Y., Jordan, M., Tenberge, P., Dong, P.: Optimized control of engine start assisted by the disconnect clutch in a p2 hybrid automatic transmission. Mech. Syst. Signal Process. **124**, 313–329 (2019)
16. Wang, F., Xia, J., Xu, X., Cai, Y., Zhou, Z., Sun, X.: New clutch oil-pressure establishing method design of phevs during mode transition process for transient torsional vibration suppression of planetary power-split system. Mech. Mach. Theory **148**, 103801 (2020)
17. Yang, C., Jiao, X., Li, L., Zhang, Y., Chen, Z.: A robust h-infinity control-based hierarchical mode transition control system for plug-in hybrid electric vehicle. Mech. Syst. Signal Process. **99**, 326–344 (2018)
18. Sato, R., Fukumoto, S.: Response-time analysis for controller area networks with randomly occurring messages. IEEE Trans. Vehic. Technol. **69**(4), 3893–3902 (2020)
19. Navet, N.: Controller area network [automotive applications]. IEEE Potentials **17**(4), 12–14 (1998)
20. Marino, A., Schmalzel, J.: Controller area network for in-vehicle law enforcement applications. In: 2007 IEEE Sensors Applications Symposium, pp. 1–5 (2007)
21. Du, L., Dao, H.: Information dissemination delay in vehicle-to-vehicle communication networks in a traffic stream. IEEE Trans. Intel. Transport. Syst. **16**(1), 66–80 (2015)
22. Luan, Z., Zhang, J., Zhao, W., Wang, C.: Trajectory tracking control of autonomous vehicle with random network delay. IEEE Trans. Vehic. Technol. **69**(8), 8140–8150 (2020)
23. Liu, Y., Zhu, X., Zhang, H., Basin, M.: Improved robust speed tracking controller design for an integrated motor-transmission powertrain system over controller area network. IEEE/ASME Trans. Mechatron. **23**(3), 1404–1414 (2018)
24. Zhu, X., Zhang, H., Wang, J., Fang, Z.: Robust lateral motion control of electric ground vehicles with random network-induced delays. IEEE Trans. Vehic. Technol. **64**(11), 4985–4995 (2015)
25. Liang, C., Xu, X., Wang, F., Zhou, Z.: Coordinated control strategy for mode transition of dm-phev based on mld. Nonlinear Dyn. **103**(1), 809–832 (2021)
26. Zhang, X., Liu, H., Zhan, Z., Wu, Y., Zhang, W., Taha, M., Yan, P.: Modelling and active damping of engine torque ripple in a power-split hybrid electric vehicle. Control Eng. Pract. **104**, 104634 (2020)
27. Tindell, K., Burns, A., Wellings, A.: Calculating controller area network (can) message response times. IFAC Proceed. Vol. **27**(15), 35–40 (1994)
28. Caruntu, C.F., Lazar, M., Gielen, R.H., van den Bosch, P., Di Cairano, S.: Lyapunov based predictive control of vehicle drivetrains over can. Control Eng. Pract. **21**(12), 1884–1898 (2013)
29. Shuai, Z., Zhang, H., Wang, J., Li, J., Ouyang, M.: Combined afs and dyc control of four-wheel-independent-drive electric vehicles over can network with time-varying delays. IEEE Trans. Vehic. Technol. **63**(2), 591–602 (2014)

30. Hetel, L., Daafouz, J., Iung, C.: Stabilization of arbitrary switched linear systems with unknown time-varying delays. IEEE Trans. Autom. Control **51**(10), 1668–1674 (2006)
31. Li, P., Nguyen, A.T., Du, H., Wang, Y., Zhang, H.: Polytopic lpv approaches for intelligent automotive systems: State of the art and future challenges. Mech. Syst. Signal Process. **161**, 107931 (2021)
32. Boyd, S., El Ghaoui, L., Feron, E., Balakrishnan, V.: Linear Matrix Inequalities in System and Control Theory, Studies in Applied Mathematics, vol. 15. SIAM, Philadelphia, PA (1994)
33. de Oliveira, M., Bernussou, J., Geromel, J.: A new discrete-time robust stability condition. Syst Control Lett **37**(4), 261–265 (1999)
34. Palacios-Quiñonero, F., Rubió-Massegú, J., Rossell, J., Karimi, H.: Feasibility issues in static output-feedback controller design with application to structural vibration control. J. Franklin Inst. **351**(1), 139–155 (2014)
35. Meng, Q., Qian, C., Sun, Z.Y., Chen, C.C.: A homogeneous domination output feedback control method for active suspension of intelligent electric vehicle. Nonlinear Dyn. **103**(2), 1–18 (2021)
36. Meng, Q., Xu, H., Sun, Z.Y.: Nonlinear lateral motion stability control method for electric vehicle based on the combination of dual extended state observer and domination approach via sampled-data output feedback. Trans. Inst. Measur. Control **43**(10), 2258–2271 (2021)